Case Studies in Thermal Engineering 53 (2024) 103911

Contents lists available at ScienceDirect

Case Studies in Thermal Engineering

journal homepage: www.elsevier.com/locate/csite

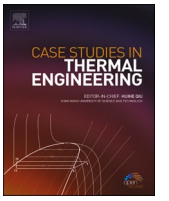

Downsizing strategy for an air-cooled indirect-fired single-effect ammonia-water absorption chiller in part-load operation in hot climates

María Esther Palacios-Lorenzo *, José Daniel Marcos

Dept. of Energy Engineering, UNED, Juan del Rosal 12, 28040, Madrid, Spain

ARTICLE INFO

Keywords:
Downsizing
Thermodynamics
Ammonia-water
hot climate
Absorption
Gax

ABSTRACT

A modular mathematical model has been created to simulate an ammonia-water absorption refrigeration system indirectly fired and air-cooled. The model includes governing equations based on mass, species, and energy balances, implemented for the main components of the system. It accounts for both thermal and mass resistances in the transfer processes that occur in the system. The study evaluates the performance of the ROBUR® absorption refrigeration system, model ACF60-00 LB, operating under part-load conditions, driven by hot water temperatures ranging between 160 and 210 °C, while the ambient temperature remains up to 40 °C. This refrigeration system is characterised by including an extra valve that allows active control of the pressure levels of the system. The analysis focusses on the effect of its active control on the size of the system. The results show that increasing the pressure loss in this valve reduces the size of the air-cooled absorber to 37.3 % of its nominal size at an ambient temperature of 40 °C, while the reduction in refrigerant mass flow is 18.5 %, while the condenser size decreases 3.1 times. Evaporator, air-cooled absorber and condenser effectiveness are minimally affected. Additionally, contribution of condenser and evaporator to exergy destruction is balanced.

1. Introduction

The development of markets and climate change has led to an increase in electricity demand of approximately 60 % at the beginning of 2030 [1]. Meeting peak requirements poses challenges in transitioning away from fossil fuels due to concerns about energy security. Solar energy stands out as a promising alternative because it aligns, to some extent, with peak load patterns. In Europe, prioritising solar heat as a key element for sustainable cooling is a goal (Solar Heat Europe). Absorption technology, which can be driven by thermal solar energy, represents an environmentally friendly option compared to conventional compression systems [2]. Among the conventional working fluids for absorption chillers, the pair stands out due to its ability to provide cooling below zero, making it suitable for refrigeration, along with its wide feed temperature range [3] and the absence of crystallisation, particularly at high environmental temperatures [4]. Ammonia-water (NH_3–H_2O) absorption refrigeration systems have applications not only in the refrigeration sector but are also effectively used for desalination purposes [5,6] in hybrid configurations, what may contribute to solving water scarcity concern associated to the climate change. This context is part of the European ASTEP project, in which our current work is framed. The primary objective of this project is to analyse the feasibility of using solar energy to meet the cooling demands of the dairy industry in Greece. For this purpose, a rotating Fresnel collector was developed [7], which supplies hot water to a

* Corresponding author.
E-mail address: epalacios@ind.uned.es (M.E. Palacios-Lorenzo).

https://doi.org/10.1016/j.csite.2023.103911
Received 31 August 2023; Received in revised form 30 November 2023; Accepted 10 December 2023
Available online 21 December 2023

commercial air-cooled NH_3/H_2O absorption system.

Numerous studies have been conducted to optimize the performance of single-stage absorption cooling systems [8], such as water ammonia chillers assisted by compressors and ejectors [9,10]. Both strategies involve changing the pressure level of the air-cooled condenser (ejector-assisted) or absorber (compressor-assisted). New fluid mixtures have also been investigated to address some weaknesses in the NH_3/H_2O pair, such as improving thermal conductivity [11] and increasing the boiling temperature differences [12]. However, the pair remains widely used in commercial absorption systems operating below zero [13].

Absorption cooling systems require heat rejection systems, traditionally employing wet cooling towers. However, this approach has drawbacks, including water consumption, the risk of Legionella bacteria, and low efficiency in humid climates, prompting the exploration of alternative solutions. Direct air-cooled absorption chillers do not require water consumption but suffer from high thermal resistance. Air-cooled absorbers and condensers often use air-cooled fin-and-tube designs [14], known for their limited compactness. To address this issue, conventional finned tubes in the condenser can be replaced by mini/micro finned coils [15], which also help reduce the refrigerant charge of the chiller [16]. However, the compactness of the chiller can compromise its efficiency [17], especially in air-cooled refrigeration systems.

Absorbers have been extensively studied, as they are considered to be the bottleneck of absorption chillers. Ferreira [18] found that the size of the absorber primarily affects the cooling capacity of the machine. The flow pattern in air-cooled absorbers significantly influences the local and mass transfer coefficients on the side of the liquid solution [19,20]. The dominant thermal resistance in air-cooled direct absorbers is on the air side [21,22]. An optimal tube diameter that reduces the absorber length has also been identified. Goyal et al. [14] identified limitations in heat transfer within the absorber caused by the decrease in driving temperature difference and overall thermal conductance. To address these issues, they proposed modifying the absorber by augmenting heat transfer coefficients on the tube side and increasing the surface area, which would alleviate the reduction in overall system performance ([14,23,24]). Chakraborty et al. [25] investigated the efficacy of a new multi-pass tube-array condenser as compared to a traditional round-tube corrugated fin condenser. It has been demonstrated that thermal external resistance can be decreased by increasing the number of fins in the condenser's rows as well as by increasing the air-flow rate. Furthermore, the use of tubes with smaller diameters led to a reduction in internal resistance.

It is known that the combined analysis of energy and exergy can provide a precise identification of irreversible sources. However, only a few studies include the evaluation of chemical exergy in the analysis [26,27]. In the latter, ambient pressure is chosen as the dead-state condition, although this choice is not logical for closed refrigeration cycles [28].

This study focusses on downsizing the single effect indirect-fired air-cooled NH_3/H_2O absorption chiller during partial load operation. The case study considers the downsizing of the Robur® absorption chiller, model ACF60-00 LB, powered by hot water, when used for cooling purposes in the dairy industry. The strategy that will be analysed involves controlling pressure loss of an additional valve, which is a characteristic of the Robur® absorption chiller, to act on both high and low pressure levels of the absorption system during off-design operation. The study examines the impact of the driving temperature difference on the heat transferred across the evaporator, absorber and condenser, for a given geometry of these components. It considers the limitations due to the size of the refrigerant absorption chiller.

A differential mathematical model has been developed and implemented, based on equations developed by Colburn and Drew, incorporating local heat and mass transfer coefficients. The variation of the thermal transmittance at part load conditions is also considered by the model [29].

The novel of this study can be summarized as follows:

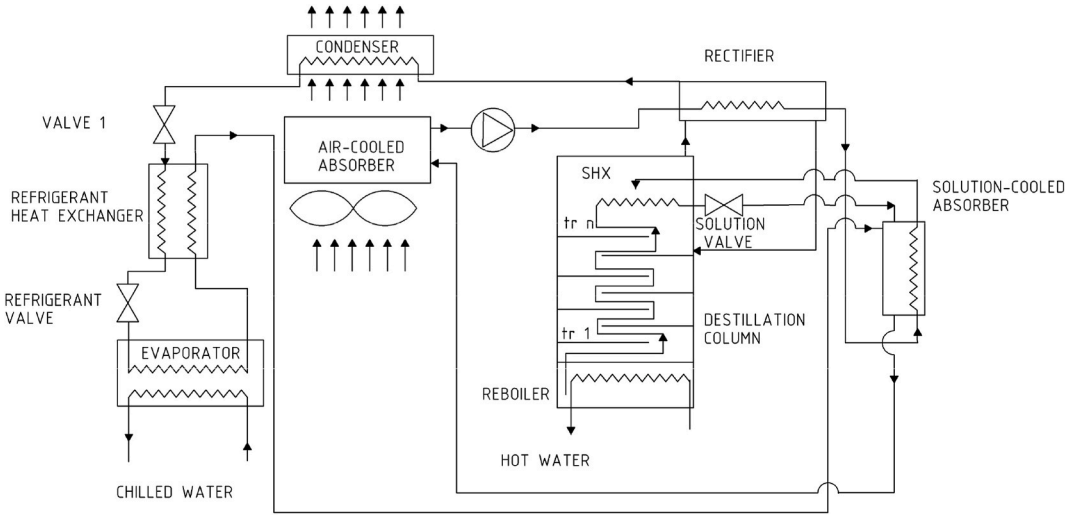

Fig. 1. Flow diagram of the ROBUR absoption chiller model ACF60-00 LB.

- The utilization of the pressure loss from a valve located immediately downstream of the condenser in the refrigeration flow side, a distinctive feature of the Robur® absorption chiller, as a strategy for downsizing the air-cooled ammonia-water absorption chiller.
- A methodology for analysing the modified gax-cycle characteristic of the Robur® absorption chiller and determine the minimum size of the air-cooled absorber and condenser, in series configuration, when the chiller operates at part load under this strategy.

The main results show that the strategy analysed leads to acting on the high and low pressure levels. As a result, the size of the absorber is reduced. Refrigerant mass flow is also reduced, but to a lesser extent. The size of the condenser is significantly reduced, which contributes to exergy destruction. However, this is offset by the reduced contribution of the evaporator. The proposed strategy effectively downsizes the chiller.

2. Analysis

2.1. Description of the absorption chiller

The absorption chiller considered in this work is shown in Fig. 1, while Table 1 provides detailed information on the geometry of the various components that comprise the chiller. The purification system aims to achieve a vapour refrigerant with the required purity [30], and consists of the distillation column and the solution-cooled rectifier at the top, to achieve a vapour refrigerant with the required purity. The distillation column includes only the stripping section due to the lack of significant advantages associated with a rectifying section, coupled with the decrease in COP [31]. A solution-cooled absorber allows for the recovery of some of the absorption heat [32]. The chiller incorporates two valves: refrigerant and solution valve, which enable re-establishment of the low-pressure level at the inlet of the solution pump. Additionally, the refrigeration system features an additional valve, called valve 1, located immediately downstream of the condenser, which allows the adjustment of the pressure level of the refrigeration system. This study analyses the impact of active control of pressure loss in valve 1 to reduce the size of the absorption system. In addition, it investigates the efficiency and performance of the refrigeration absorption system.

The condenser, air-cooled absorber and evaporator tubes are described by their inner diameter, *Di,* thickness, *e*, and number of tubes. The evaporator is a baffled shell and tube heat exchanger. The refrigerant quality at the exit of the evaporator is fixed at 0,96 to limit the temperature glide. Both the solution-cooled absorber and the solution-cooled rectifier are helical tubes, which have different numbers of turns, N_{turns}. The refrigeration heat exchanger is modelled with a constant efficiency of 0,9. The geometry of the distillation column, of tray type, is defined by its inner diameter D_i, hole diameter, d_h = 0,00381 m, tray thickness, e_{tray}, tray spacing, S_t, weir length, l_w, hole pitch, $s_h = 3\ d_h$, weir height, h_w, and two relationships, $A_d/A_t = f(l_w/D_i)$ and $A_h/A_a = g(d_h/s_h)$ [33], being $A_t = \pi/4\ D_i^2$, A_d, and $A_a = A_t$ - $2A_d$, the column area, the downcomer area and the active area, respectively. The reboiler is an annular cylinder equipped with annular fins. The geometry of the finned surface for the condenser, absorber, and reboiler annuli is determined by the thickness, t_m, and pitch, s, of their fins.

2.2. Model development

The implementation of the mathematical model in the engineering equation solver (EES) software is structured with separate modules for each key device in the Robur® absorption refrigeration system. Thermodynamical properties have been evaluated according to Ibrahim and Klein [34]. Each module incorporates the mathematical model developed based on the principles of conservation of mass, species, and energy applied to the individual differential volumes that make up the modelled device.

$$\sum_i \dot{m}_{\ in} - \sum_i \dot{m}_{\ out} = 0 \tag{1}$$

$$\sum_i (x \bullet \dot{m})_{\ in} - \sum_i (x \bullet \dot{m})_{\ out} = 0 \tag{2}$$

Table 1
Geometry of the main components of the absorption chiller.

Condenser/air-cooled absorber		Rectifier/solution cooled absorber		Evaporator	
D_i [m]	0,02	D_{to} [m]	0,075	D_i [m]	0.015
t_m [m]	0,0002	D_{ti} [m]	0,045	e [mm]	0.002
s [m]	0,003	D_{wi} [m]	0,0065	s [m]	1,15($D_i + e$)
e [m]	0.002	*e [m]*	0,002	N_{tube}	35
N_{tube}	2	$N_{turns\ rect}$	40	$D_{i,shell}$ [m]	(N_{tube} +1) s
		$N_{turns\ cabs}$	16	L [m]	1,1

Reboiler		Distillation column	
h_f [m]	0,63	D_i [m]	0,075
t_m [m]	0,0004	A_d [m^2]	0,12 A_t
s [m]	0,003	S_t [m]	0,15
		h_w [m]	0,1 S_t
		e_{tray} [m]	0,003

$$\sum_i (h \bullet \dot{m})_{in} - \sum_i (h \bullet \dot{m})_{out} + \dot{Q}_i = 0 \tag{3}$$

$\dot{m}$, x, h refers to the mass flowrate, mass fraction and enthalpy of the flow. The heat transfer interaction of the control volume, $\dot{Q}_i$, is modelled by the Newton's law of cooling

$$\dot{Q}_i = h_t A_i \frac{(T_i - T_w) - (T_{i+1} - T_w)}{ln\left(\frac{T_i - T_w}{T_{i+1} - T_w}\right)} \tag{4}$$

where h_t refers to the local heat transfer coefficient and A_i is the heat transfer area of the control volume. The thermal conductance of every device is calculated in each operating condition to improve accuracy in the off-design operation [29]. The flow rate of the pumped solution is kept constant under all working conditions [35]. The air-facing cooling velocity is also kept constant. The following assumptions have been considered:

- The processes are in steady state.
- Pressure drops are only considered through the valves.
- The dilute solution leaving the reboiler is at saturated state.
- The refrigerant leaving the condenser and the evaporator is at saturated state.
- The effectiveness of the refrigerant heat exchanger is constant.
- Heat losses to the environment are negligible.
- Flow is one-dimensional.
- Heat and mass are transferred radially through the tube.
- The ammonia mass fraction in the solution remains constant across all working conditions.

2.2.1. Distillation column module

The distillation column in the Robur® absorption refrigeration system is discretised into trays, which enables a detailed analysis of the distillation process. The reboiler and the solution-cooled rectifier are also treated as additional trays to assess the heat flow transferred during partial condensation in the rectifier and the vapour generation in the reboiler.

To evaluate the efficiency of each vapour plate (tray) in the distillation column, the Murphree vapour plate efficiency (e_M) is calculated. The Murphree efficiency of the vapour plate provides a measure of the efficiency with which the tray accomplishes the separation of the components in the vapour phase. In this case, the Wilke-Chang approach [33] is used to calculate the ammonia molar fraction of the vapour that leaves each tray. The Wilke-Chang approach is a well-known correlation that is used to estimate the vapour-liquid equilibrium for mixtures. Thus, the ammonia molar fraction of the vapour leaving the i-tray, $\overline{x}_{v,i}$, is obtained as,

$$\overline{x}_{v,i} = \overline{x}_{v,i-1}(1 - e_M) + e_M \overline{x}_{v\ e,i} \tag{5}$$

where $\overline{x}_{v\ e,i}$ refers to the molar mass fraction of the vapour in thermodynamic equilibrium that leaves the i-tray. The effect of liquid entrainment has also been considered using the Fair method [33]. For simplicity, the interaction between the liquid coming from the reboiler and the vapour flow is ignored.

2.2.2. Modules for evaporator, condenser and reboiler

The evaporator and condenser are discretised in differential control volumes, which include two different regions: the refrigeration side and the coolant side. Only one control volume is considered in the reboiler module, which encloses the solution side and the hot water side to calculate the transferred heat flow. To accurately assess the heat transfer coefficient ($h_{t,\ ref}$) of the zeotropic refrigerant mix (ammonia-water mixture) on the refrigeration side, the Silver andBell andGhaly approach is used:

$$h_{t,ref} = h_{t,pure} \Big/ (1 + K)^4 \tag{6}$$

where $h_{t,pure}$ is the heat transfer coefficient based on the pure fluid model using mixture properties. The correction factor, K, is evaluated by Ref. [36]. The Silver and Bell andGhaly approach is a correlation that is used to estimate the heat transfer coefficients in zeotropic mixtures under specific conditions.

2.2.3. Modules for air-cooled absorber, solution-cooled absorber, and rectifier

In the mathematical model, each device in the Robur® absorption refrigeration system is discretised into differential control volumes, which further divide the device into four distinct regions: the vapour side, the liquid solution side, the vapour-liquid interface, and the coolant side. This level of discretization allows for a detailed analysis of the mass, species, and energy balances at the interface between the vapour and liquid phases within each control volume.

At the vapour-liquid interface of each control volume, the mass, species, and energy balance equations are established. These equations account for the transfer of mass and energy between the vapour and liquid phases, which is crucial for accurately modelling the absorption refrigeration process.

To determine the ammonia molar flux from the vapour to the liquid interface, the expression proposed by Bird [21] is used:

$$\dot{n}_{NH_3,v} = F_v \bullet z \bullet ln\left(\frac{z - x_{vi}}{z - x_v}\right) \tag{7}$$

where F_v is the mass transfer coefficient of the vapour, z is the ratio of ammonia to total molar flux, x_v is the molar mass fraction of the vapour. Subscript i refers to the thermodynamic equilibrium state. Local mass and thermal transfer coefficients are applied. Accordingly, the ammonia molar flux transferred from the interface to the bulk liquid is evaluated as:

$$\dot{n}_{NH_{3,L}} = F_{Li} \bullet z \bullet ln\left(\frac{z - x_L}{z - x_{Li}}\right) \tag{8}$$

where F_{Li} is the mass transfer coefficient of the liquid at the interface. The mass conservation balance at interface states that $\dot{n}_{NH_{3,L}}$ to be equal to $\dot{n}_{NH_{3,v}}$. In addition, the energy conservation requirement at the interface is established by:

$$\dot{Q}_L = \dot{Q}_v + \dot{m}_{NH_3}\, \Delta h_{NH_3} + \dot{m}_{H_2O}\, \Delta h_{H_2O} \tag{9}$$

where $\dot{Q}_L$ and $\dot{Q}_v$ are the heat flow transferred from the vapour to the interface and from the interface to the liquid phase, respectively. Δh refers to the difference between the partial enthalpies of vapour and liquid at the interface. An iterative process allows one to calculate the mass and heat flow rate transferred at the interface in each control volume, the heat and mass transfer interface area of each differential control volume, A_i, given by:

$$A_i = a_{int} \frac{\pi D_i^2}{4} \Delta x \tag{10}$$

with a_{int} refers to the specific interfacial area.

2.2.4. Evaluation of the exergy destruction

The exergy destruction in an elemental volume is evaluated with the balance of exergy, where the total intensive exergy associated with a material flow, e_i, is divided into its mechanical and chemical parts. Mechanical part is evaluated as

$$e_i^{PH} = h_i - h_{i,0} - T_0\left(s_i - s_{i,0}\right) \tag{11}$$

The point 0 to calculate the physical exergy dependent on the reference ambient temperature, $T_0 = 25\ ^\circ C$, and the pressure within the refrigeration system when the absorption system is not in operation, P_0, [28]. The chemical part is calculated as [37].

$$e_i^{CH} = x_i \bullet e_{NH3}^{CH} + (1 - x_i) \bullet e_{H2O}^{CH} + w_{xi}^{mix} \tag{12}$$

where w_{xi}^{mix} is the specific work associated with the mixing of pure refrigerant (NH_3) and pure absorber (H_2O)

$$w_{xi}^{mix} = \left[h_{j0} - x_i \bullet h_{NH3,0} - (1 - x_i) \bullet h_{H2O,0}\right] - T_0\left[s_{j0} - x_i \bullet s_{NH3,0} - (1 - x_i) \bullet s_{H2O,0}\right] \tag{13}$$

For an absorber refrigeration system, it is considered that $e_{H2O}^{CH} = 45$ kJ/kmol and $e_{NH3}^{CH} = 336\ 684$ kJ/kmol

2.2.5. Evaluation of the heat and mass transfer coefficients

In the mathematical model implemented for the Robur® absorption refrigeration system, various heat transfer and mass transfer coefficients are calculated using different correlations and approaches for each specific component. Here is a summary of the methods used for each device:

- Reboiler: The correlation proposed by Gorenflo [38] is used to calculate the heat transfer coefficient on the solution side. The heat transport coefficient between the wall of the reboiler finned tube and the coolant is obtained from Ref. [39].
- Evaporator: The heat transport coefficient between the tube wall and the coolant in the evaporator is calculated following the procedure described in Ref. [39] for the heat transfer in the baffled shell and the tube heat exchangers. On the solution side, the Klimenko correlation [38] is used to evaluate the heat transfer coefficient.
- Solution-cooled absorber and rectifier: The heat transfer coefficient between the liquid and the tube surface is determined by using film-wise condensation theory in a horizontal tube. In the laminar regime, the heat transfer coefficient is obtained from the Nusselt equation for a smooth film [39]. Increase in heat transfer due to the waviness of the film flow is considered using the Kutateladze and Gogonin equation [39]. In the turbulent regime, the Yüksel and Müller equation [39] is used to calculate the heat transfer coefficient. Corrections proposed by the Numrich equations [39] are applied to account for the effect of shear stress on the film

Table 2
Mass and heat transfer coefficients.

regime		Mass transfer coefficient	Heat transfer coefficient
intermittent	Liquid to interface	Scott & Hayduk [49]	Film wise condensation [39]
stratified	Liquid to interface	Scott & Hayduk [49]	Film wise condensation [39]
bubble	Liquid to interface	Ciborowski & Rychlicki [50]	Film wise condensation [39]
–	Vapour to interface	Chilton & Colburn analogy [39]	Gnielinski [39]

surface in both the laminar and turbulent regimes. The mass transfer coefficient is evaluated with the Chilton & Colburn analogy [39].

- Condenser and air-cooled absorber: the heat transfer coefficient on the air-coolant side is evaluated by the correlation proposed by Qasem et al. (2008) [40].
- Air-cooled absorber: the flow pattern is calculated as reported by Ref. [41]. In the intermittent regime, the void fraction [42–45], the bubble velocity in the slug [46], and the bubble length [47] are evaluated. In the stratified regime, the void fraction is calculated using the Armand-Massina correlation [48]. The mass and transfer coefficients are detailed in Table 2

2.3. Solution methodology

The solution method considers as invariant quantities for each operating condition, in addition to the chiller geometry, as detailed

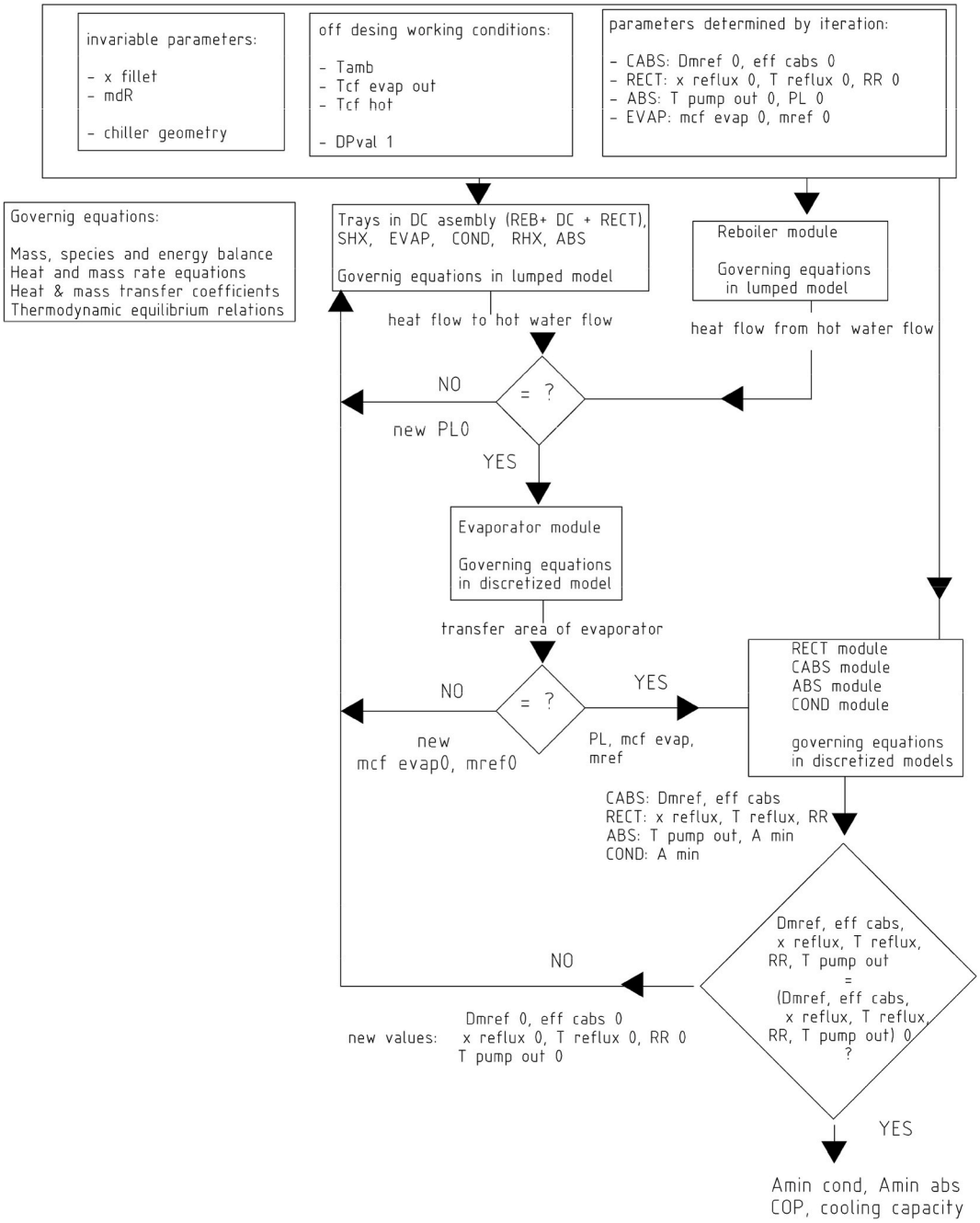

Fig. 2. Simplified Model diagram.

in Table 1, the mass fraction of the fillet solution, x_{fillet}, when the machine is at standstill, and the mass flow rate of the pumped solution, $\dot{m}_{dP}$. For each operating condition of the absorption system (determined by T_{amb}, $T_{cf\ hot}$, and $\dot{m}_{cf,reb}$), $\Delta P_{valv\ 1}$ is arbitrarily set in order to manage the high pressure level, P_H. The chilled water mass flowrate, $\dot{m}_{cf,evap}$, is considered as a variable quantity, as indicated by the manufacturer's data, which specifies a certain range of variation. Therefore, its value is evaluated for each operating condition. Fig. 2 shows a simplified flow chart of the model.

A number of parameters, marked with 0 in Fig. 2, are initially estimated and iteratively determined by the mass, species, and energy balance using heat and mas transfer coefficients. In particular, the low pressure level, P_L, the flow of the chilled water $\dot{m}_{cf,evap}$, and the heat flow from the hot water flow, $\dot{m}_{cf,reb}$, are determined by matching the heat flow from the hot water flow, $\dot{m}_{cf,reb}$, with the one to the solution at the reboiler after checking that the evaporator be able to carry out the completeness of the evaporation process.

The iterative process of integrating each unit into the absorption chiller is summarized in the flow diagram in Fig. 4. The calculation procedure follows the following steps:

1. Guess the refrigerant mass fraction, $x_{ref\ 0}$, the low-pressure level, P_{L0}, the refrigerant mass flow rate $\dot{m}_{ref0}$, the temperature of the solution at the pump outlet, $T_{pump\ out}$, the effectiveness of the solution-cooled absorber, ε_{cabs}, the reflux ratio, R, the temperature, and mass fraction of the condensate at the rectifier outlet, T_R and x_R respectively.
2. Run the main module of the mathematical model. The high pressure level, P_H, the reboiler heat flow, $\dot{Q}_{reb}$, and the absorbed refrigerant mass flow rate in the solution-cooled absorber, $\Delta\ \dot{m}_{ref,cabs}$ is calculated.
3. Run the re-boiler module. Check $\dot{Q}_{reb}$. If verified, go to step 4. Otherwise, guess a new value of $\dot{m}_{ref}$ and go to step 2.
4. Run the evaporator module. Check the refrigerant flow rate at the evaporator outlet. If verified, go to Step 5. Otherwise guess a new value of $\dot{m}_{cf,evap}$, or guess a new value of P_L, and go to Step 2
5. Run the rectifier module. Check RR, T_R, x_R and $N_{turns\ rect}$. If verified, go to Step 6. Otherwise, guess new values of RR, T_R, x_R, and go to Step 2.
6. Run the solution-cooled absorber module. Check $N_{turns,\ cabs}$ and ε_{cabs}. If verified, go to Step 7. Otherwise, guess a new value of ε_{cabs} and go to Step 2.
7. Run the air-cooled absorber module. The minimum area of the air-cooled absorber required to ensure the completeness of the absorption process, and the $T_{pump\ out}$ value are calculated. Check $T_{pump\ out}$. If verified, go to Step 8. Otherwise, guess a new value of $T_{pump,out}$ and go to Step 2.
8. Run the condenser module. The minimum area of the condenser required to ensure the completeness of the condensation process is calculated.

2.4. Model validation

In the present study, an air-cooled indirect fired ammonia-water absorption refrigeration system is examined for ambient temperature ranging from 15 to 40 °C, when generating chilled water at −5 °C. The precision of the proposed modelling is carried out based on the manufacturer's data on the ROBUR® absorption refrigeration system, model ACF60-00 LB, and the experimental data of the air-cooled ROBUR® absorption system reported in Ref. [32], although the latter are based on a direct-fired system.

No information is available on the pressure loss in valve 1, apart from the value reported in Ref. [30], based on an indirect-fired air-cooled ROBUR® absorption system. It should be noted that in this case, the system operates for air conditioning purposes. Additional information is provided by the numerical model reported in Ref. [51], based on a direct-fired ROBUR® absorption system, when operating for air conditioning purposes.

Therefore, there is a lack of detailed experimental data to validate the accuracy of the proposed modelling. To solve this problem, a baseline configuration is defined with ΔP_{valv1} set at 175 kPa and $T_{cf,hot}$ at 160 °C. Fig. 3a shows that the cooling capacity and COP agree well with the manufacturer's data. On the other hand, the high and low pressure levels in the refrigeration system are validated with the experimental data reported in Ref. [35]. Fig. 3b shows that the model is in good agreement with the experimental results.

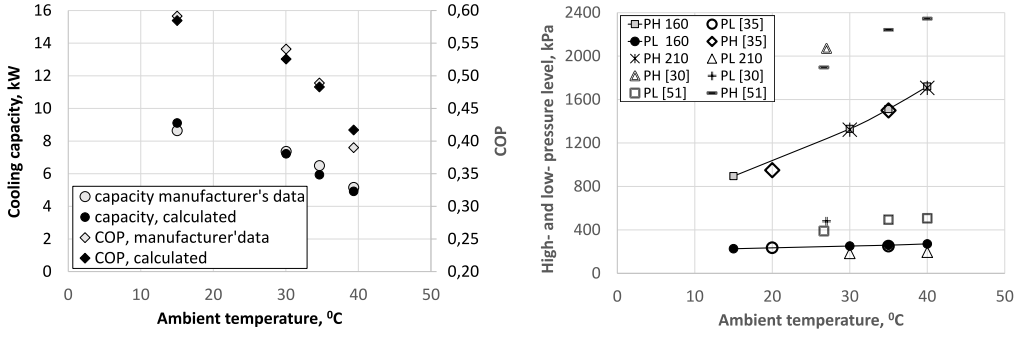

Fig. 3. a) Cooling capacity and coefficient of performance, b) high and low pressure levels, P_H and P_L, respectively. $\Delta P_{valv1} = 175$ kPa, $T_{cf,hot} = 160$ °C.

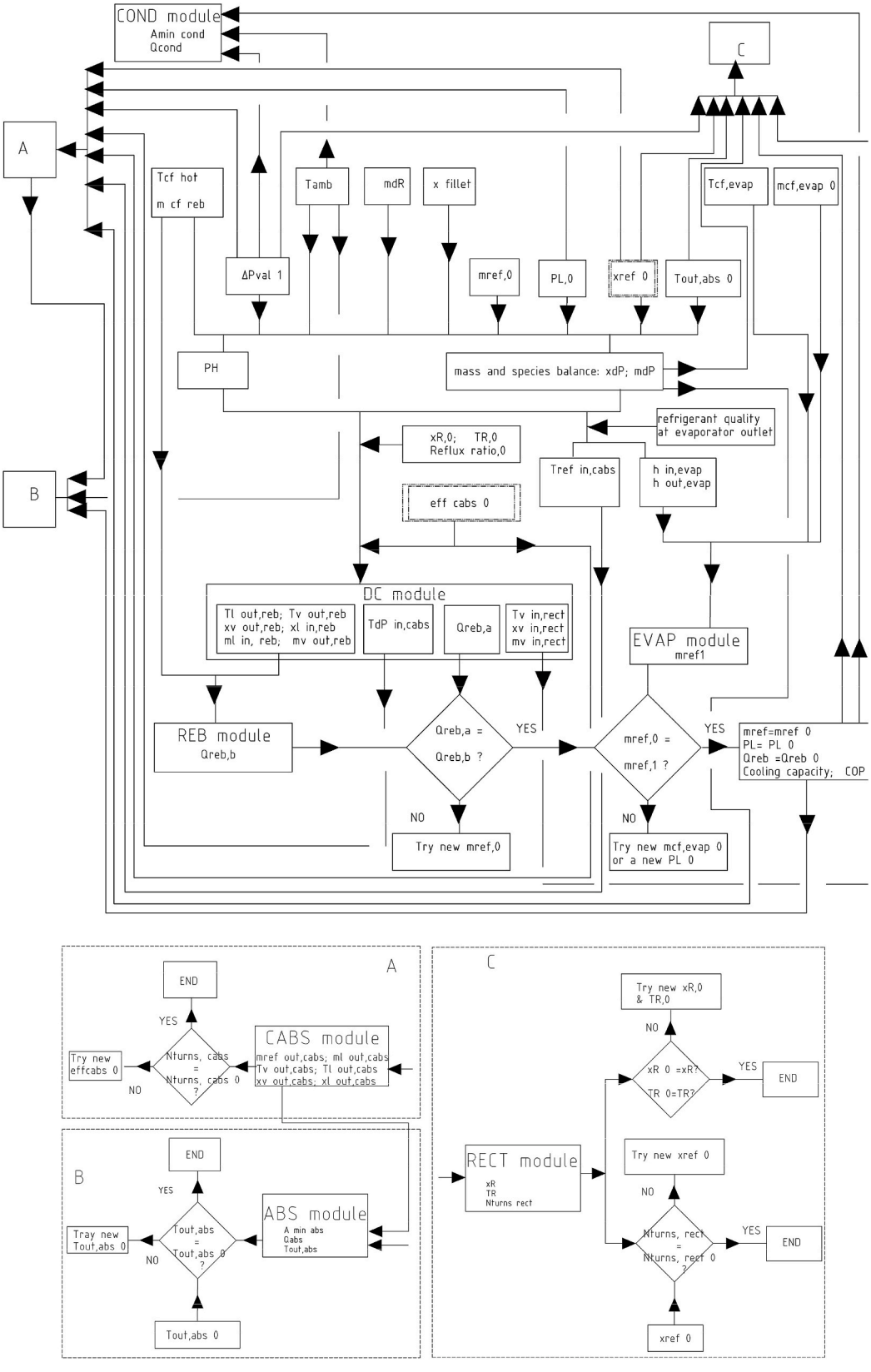

Fig. 4. Model diagram.

3. Results

The values reported in Refs. [30,51] for the low pressure level are higher than those indicated in Ref. [32] (Fig. 5a). This is attributable to the fact that the latter operates for refrigeration purposes and not for air conditioning, as the first two. Furthermore, the values for the high pressure level reported in Refs. [30,51] are noticeably higher than those reported in Ref. [35], which would deteriorate the performance of the system [17].

Fig. 4b shows the high and low pressure levels according to the modelling, with ΔP_{valv1} set at 175 kPa. Note that the low pressure level decreases even further when the $T_{cf\ hot}$ increases from 160 to 210 °C, which could compromise the performance of the air-cooled absorber, particularly at high ambient temperature. Furthermore, the high pressure level does not change as the $T_{cf\ hot}$ temperature increases, so an increase in the $T_{cf\ hot}$ temperature seems to justify the very high P_H values reported in Refs. [30,51] compared to those in Ref. [35].

In view of this, it is interesting to analyse the effect of ΔP_{valv1} on the absorption refrigeration system. Therefore, a customised configuration has been defined for $T_{cf\ hot} = 210$ °C, the feedwater temperature for which the coolant flow rate generated is the highest in the range provided by the manufacturer. For this configuration, the value of ΔP_{valv1}, denoted by ΔP_{valv1L}, has been calculated for each ambient temperature value, using modelling, such as the calculated COP and the cooling capacity of the chiller to be in good agreement with the ones provided by the manufacturer. Therefore, ΔP_{valv1L} can be expressed as $\Delta P_{valv1L} = f\ (T_{amb},\ T_{cf\ hot} = 210\ °C)$.

Fig. 5 shows the effect of ΔP_{valv1L} on the high and low pressure levels. Note that the P_H obtained by the modelling is close to that reported in Refs. [30,51], specially at T_{amb} of 40 °C. However, the P_L is still significantly lower compared to Refs. [30,51], which is since absorption chillers analysed in Refs. [30,51] operated for air conditioning purposes.

Table 3 illustrates how $\Delta P_{val\ 1}$ affects high and low pressure levels. P_H increases as expected with $\Delta P_{val\ 1}$ when $T_{cf,hot}$ remains constant. Note that P_L also increases due to the decline in cooling capacity. Consequently, P_L decreases with an increases in $T_{cf,hot}$. The results show a 10.49 % increase in P_L of when $\Delta P_{val\ 1}$ goes up from 175 kPa to ΔP_{val1L}, at $T_{amb} = 40$ °C.

Next, the effect of increasing ΔP_{valv1} on the size and performance of the air-cooled assembly is explored. Firstly, the effect of ΔP_{valv1} on the performance of the evaporator is analysed. Finally, the impact of the size of the refrigerant system on the exergy cost is assessed.

3.1. Evaporator

Table 4 illustrates that the circulation ratio, f, increases by 18.3 % at $T_{amb} = 40$ °C, as the pressure drop ΔP_{val} rises by 75 %, following the reduction of $\dot{m}_{ref}$. This is caused by a decrease in vapour production in the reboiler. Hence, it is crucial to evade high values of $\Delta P_{val\ 1}$ at low $T_{cf\ hot}$ or maintaining f within a reasonable range in all working environments. In contrast, Table 4 shows a 68.1 % reduction in the temperature glide of the refrigerant flow, $T_{glide,ref}$, at $T_{amb} = 40$ °C, due to the increase in P_L (as indicated in Table 3). Similarly, the temperature glide of the chilled water flow, $T_{glide,\ cf.\ evap}$, also decreases. It should be noted that $T_{glide,ref}$ is not solely dependent on $\dot{m}_{cf\ evap}$ but also on $\dot{m}_{ref}$. In this study, $\dot{m}_{cf\ evap}$ was determined according to Table 5. Table 4 demonstrates a slight decrease in the thermal conductance of the evaporator, UA_{evap}, due to lowered flow rates of chilled water and refrigerant resulting from the $\Delta P_{val\ 1}$ increase. Additionally, the evaporator's effectiveness, ε_{evap}, slightly enhances.

Concerning $T_{cf,hot}$, Table 4 indicates a reverse operation of the evaporator. Fig. 6 illustrates how the circulation ratio, f, the effectiveness of the evaporator, ε_{evap}, the thermal conductance of the evaporator, UA_{evap}, and the temperature glide of the refrigerant and the chilled water flows, $\Delta T_{glide\ evap}$, $\Delta T_{glide\ cf\ evap}$, respectively, change with respect to T_{amb} and ΔP_{valv1}. It is evident from the graphic that the evaporator operates similarly when there is increase in both T_{amb} and $\Delta P_{val\ 1}$, demonstrating that $\dot{m}_{ref}$ is the primary factor affecting the evaporator's performance. Same trend was observed by Goyal et al. [14].

Consequently, the reduction in f observed in the customised configuration when compared to the baseline configuration arises from the rise in $\dot{m}_{ref}$, caused by the increase in $T_{cf,hot}$. On the other hand, the increase in $\dot{m}_{cf\ evap}$ is due to the rise in $\dot{m}_{ref}$ accompanied by the decrease in $\dot{m}_{cf\ evap}$, leading to a higher ε_{evap}. Thus, it is necessary to regulate $\dot{m}_{cf\ evap}$ for optimal tuning between $\dot{m}_{cf\ evap}$ and $\dot{m}_{ref}$.

3.2. Air-cooled components

3.2.1. Absorber

The effect of modifying the high pressure level, P_H, via $\Delta P_{val\ 1}$ control, on heat transfer in the absorber is analysed in off-design operational conditions, within limitations of size, when incorporated into an absorption chiller. Table 6 illustrates that an increase in P_L leads to an average temperature rise of 23.3 % in the local air cooling flow, $\Delta T_{cf\ abs,L}$. It is worth noting that $\Delta T_{air\ abs\ L}$ provides information on the refrigerant's absorption rate, as the cooling air-facing velocity is constant for all working conditions. Therefore, an increase in $\Delta T_{air\ abs\ L}$ implies an increase in the refrigerant's absorption rate. Furthermore, the results presented in Table 6 indicate a 6.5 % decrease in the overall airflow increase through the air-cooled absorber, referred to as $\Delta T_{cf\ abs\ G}$, at a temperature of 40 °C when $\dot{m}_{ref}$ drops by 18.5 %. The decrease of 6.5 % in $\Delta T_{cf,\ abs,G}$ aligns with the reduction of $\dot{m}_{ref}$ by 18.5 %, as mentioned above. In addition, the enhancement of $\Delta T_{cf\ abs,L}$ alongside the decrease in $\dot{m}_{ref}$, leads to a reduction of 37.3 % in the size of the air-cooled absorber, A_{abs}. Note that the decreases in $\dot{m}_{ref}$ is 18.5 %, which is less than that of A_{abs}.

Table 6 indicates that the increase of $\Delta P_{val\ 1}$ has minimal impact on the effectiveness of the air-cooled absorber, ε_{abs}. In relation to $T_{cf,hot}$, the table illustrates that the air-cooled absorber operates inversely with an increase in $\dot{m}_{ref}$ and a drop in P_L. Additionally, $\Delta P_{val\ 1}$ or $T_{cf,hot}$ have not significant effects on ε_{abs}.

Regarding T_{amb}, Fig. 7a displays the decrease of $\Delta T_{cf,\ abs,L}$ and the subsequent reduction of the refrigerant absorption rate as T_{amb} decreases. Furthermore, the figure indicates that the air-cooled absorber's minimum required area, which is normalised with its geometrical area, $A_{abs,N}$, increases as T_{amb} rises. This increase occurs despite the decrease of $\dot{m}_{ref}$ as T_{amb} rises. Nonetheless, in the

customised configuration, Fig. 6a indicates that $A_{abs,\ N}$ remains below 100 % when T_{amb} is 40 °C. Therefore, the size of the absorber is determined by the customized configuration (at $T_{cf\ hot} = 210$ °C, $T_{amb} = 40$ °C and $\Delta P_{val\ 1} = \Delta P_{val\ 1L}$). Due to the rise in P_L, the absorption rate improves as a result of the increased $\Delta T_{cf,\ abs,L.}$ In contrast, in the baseline configuration, the air-cooled absorber is oversized at $T_{cf,\ hot} = 160$ °C even though the $\dot{m}_{ref}$ has a low value at this feed temperature due to the low value of P_L.

Finally, Fig. 7b demonstrates that the absorption rate is lower at $\Delta P_{val\ 1} = 175$ kPa than at $\Delta P_{val\ 1L}$ even though the solution mass fraction is lower, when $T_{cf,hot}$ equals 210 °C. This shows that the mass fraction has a secondary influence on the performance of the air-cooled absorber.

Thus, the findings demonstrate that an appropriate increase in $\Delta P_{val\ 1}$ allows for downsizing of the air-cooled absorber while ensuring full completion of the refrigerant absorption process, even under high ambient and feed water temperatures.

3.2.2. Condenser

Table 7 presents a significant rise in the average local temperature experienced by the air-coolant flow that passes through the condenser, namely $\Delta T_{cond,L}$, upon an increase of $\Delta P_{val\ 1}$. The table shows that at a temperature of 40 °C, the condensation rate of the refrigerant flow increases by an average of 87.8 % as the $\Delta P_{val\ 1}$ rises from 175 kPa to $\Delta P_{val\ 1L}$, which is equivalent to a 75 % increase.

It should be noted that the condenser is located downstream of the absorber. Therefore, an increase in the temperature difference $\Delta T_{cf\ abs\ G}$ will have a significant impact in the effectiveness of the condenser. However, a reduction in $\dot{m}_{ref}$ occurs due to ΔP_{val1} resulting in a decline in $\Delta T_{cf\ abs\ G}$. This decrease positively affects the performance of the condenser. The results from Table 7 demonstrate an 87.8 % increase in $T_{cf,\ cond,\ L}$ when T_{amb} is at 40 °C. This results in a decrease of 90.1 % in the thermal conductance of the condenser, UA_{cond}. Consequently, the condenser's required size decreases by 316.8 %, equivalent to 3.16 times.

It has been observed that the temperature difference, $\Delta T_{cf,\ cond,G}$, decreases when the mentioned increase in $\dot{m}_{ref}$ occurs. Furthermore, the table demonstrates that $\Delta T_{cf,\ cond\ L}$ decreases by 83.1 % when $T_{cf,hot}$ increases from 160 to 210 °C, as well as the condensation rate. This is a result of the rise in $\Delta T_{cf,\ abs,G}$ and the decline in P_L, as illustrated in Table 3.

Fig. 8a and b demonstrate that the temperature difference $\Delta T_{cf\ abs\ G}$ obtains its highest levels in the customised configuration at elevated $T_{cf,hot}$, regardless of T_{amb}. However, the proposed law, ΔP_{val1L}, at $T_{cf,hot} = 210$ °C, ensures that $\Delta T_{cf\ cond\ L}$ maintains almost constant values while T_{amb} ranges between 15 and 40 °C. It is noteworthy that in the customised configuration, $\Delta T_{cf\ cond\ L}$ is higher than 3.8 °C, while $\Delta T_{cf\ cond\ L}$ barely exceeds 1.5 °C in the baseline configuration. This phenomenon is due to an increase in P_H in the customised configuration, resulting in a greater temperature difference between the condensate and the ambient temperature, as illustrated in Fig. 8c. As a result, the rate of condensation increases.

It is noteworthy that the size of the condenser is determined by the baseline configuration (at $T_{cf\ hot} = 160$ °C and $\Delta P_{val\ 1} = 175$ kPa) when $T_{amb} = 15$ °C, and $\dot{m}_{ref}$ is at its maximum. However, in the customised configuration (Fig. 8d), despite $\dot{m}_{ref}$ being 34.18 % higher, the required size of the condenser decreases to 58.2 %.

Regarding condenser effectiveness, ε_{cond}, it can be observed from Table 7 that changes in $\Delta P_{val\ 1}$ have a negligible influence on ε_{cond}. Nonetheless, upon comparing the efficiency of the condenser at different T_{amb} values for baseline and customized configurations, nearly identical results are obtained in both cases (refer to Fig. 8a and b). This implies that T_{amb} is the principal parameter influencing ε_{cond}.

3.3. Exergy cost of reduction in the size of the refrigeration system

The cost of downsizing the refrigeration system is assessed through an analysis of the exergy destruction of various components within the system. Table 8 demonstrates a mild decrease in the exergy destruction contribution of the refrigeration system, which comprises the condenser, refrigeration heat exchanger, refrigeration valves, and air-cooled solution absorber, when ΔP_{val} 1 increases from 175 kPa to $\Delta P_{val\ 1L}$. The rise in the condenser's contribution is balanced out by the reduction in the evaporator's contribution. At a temperature of 40 °C, the reduction in contribution from the refrigeration loop increases as ΔP_{val1} increases. Furthermore, when $T_{cf,\ hot}$ rises from 160 to 210 °C at 40 °C T_{amb} and $\Delta P_{val\ 1} = 175$ kPa, there is a 33 % increase in exergy destruction contribution from the refrigeration loop. As a result, the exergy efficiency of the refrigeration system is slightly decreased, consistent with the discoveries

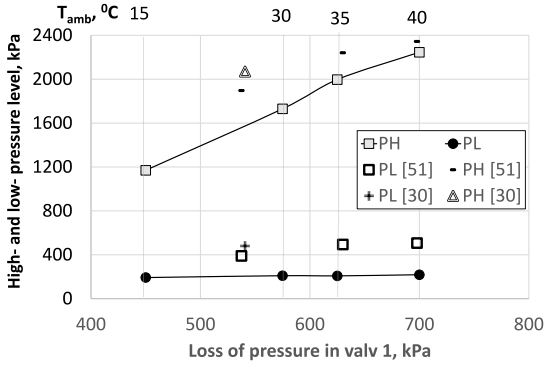

Fig. 5. High and low pressure levels, P_H and P_L. $T_{cf,\ hot} = 210$ °C.

Table 3
High- and low-pressure level. Comparative results, expressed in %.

$\Delta P_{val\ 1}$, kPa	$T_{cf,hot,}$ °C	T_{amb}, °C	$\Delta\Delta P_{val\ 1}$	ΔP_H	ΔP_L
$\Delta P_{val\ 1L}$ vs. 175	210	30	69.5	23.6	12.0
		40	75.0	24.0	10.5
175	210 vs. 160	30	0	0	−26.7
		40	0	0	−27.9

Table 4
Evaporator. Comparative results, expressed in %.

$\Delta P_{val\ 1}$, kPa	$T_{cf,hot,}$ °C	T_{amb}, °C	$\Delta\dot{m}_{ref}$	Δf	$\Delta T_{glide,\ ref}$	$\Delta T_{glide,\ cf\ evap}$	ΔUA_{evap}	$\Delta\epsilon_{evap}$
$\Delta P_{val\ 1L}$ vs. 175	210	30	−12.9	12.9	−44.7	−17.2	−1.1	1.0
		40	−18.5	18.3	−68.1	−16.6	−1.7	1.2
175	210 vs. 160	30	49.0	−49.0	43.1	55.3	3.4	13.2
		40	62.7	−62.2	26.1	61.3	7.5	12.9

Table 5
Chilled water flowrate.

T_{amb}, °C	$T_{cf,hot}$, °C	$\dot{m}_{cf\ evap}$, kg/s
15	160	3800
	210	3500
30	160	2900
	210	2500
35	160	2500
	210	2200
40	160	2000
	210	2000

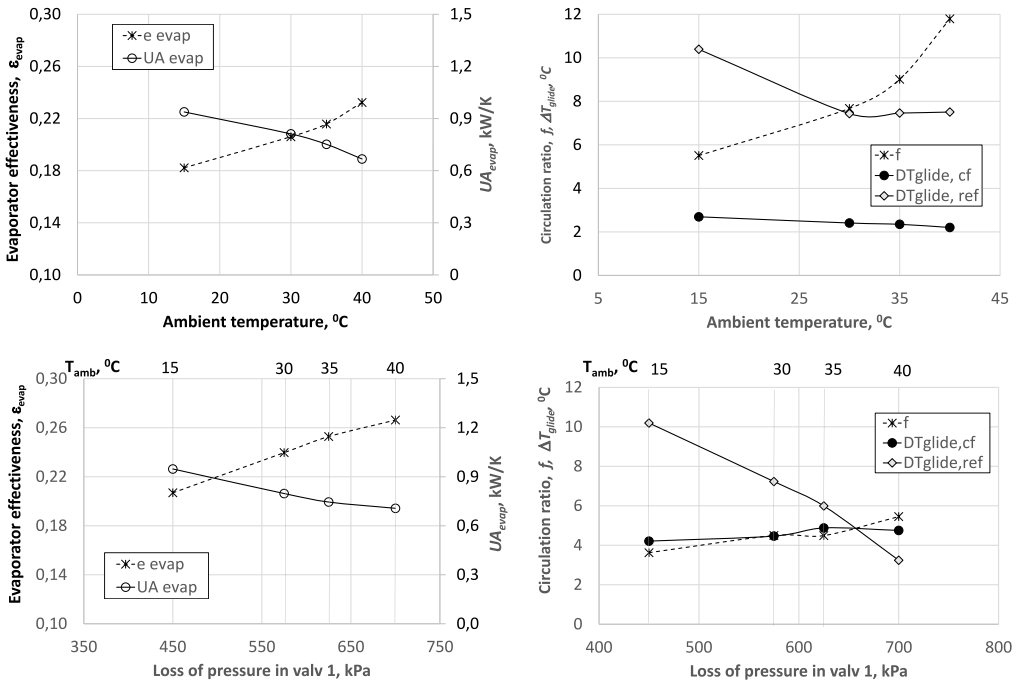

Fig. 6. Evaporator: a) effectiveness and thermal conductance, b) circulation ratio, temperature glide of the refrigerant and the chilled water in baseline configuration; c) effectiveness and thermal conductance, d) circulation ratio, temperature glide of the refrigerant and the chilled water in the customised configuration.

Table 6
Air-cooled absorber. Comparative results, expressed in %.

$\Delta P_{val\ 1}$, kPa	$T_{cf,hot,}$ °C	$T_{amb,}$ °C	$\Delta\dot{m}_{ref}$	$\Delta\Delta T_{cf\ abs,L}$	$\Delta\varepsilon_{abs}$	$\Delta\Delta T_{cf,\ abs,G}$	ΔUA_{abs}	ΔA_{abs}
$\Delta P_{val\ 1L}$ vs. 175	210	30	−12.9	41.2	0	−7.4	−13.7	−8.5
		40	−18.5	23.3	0	−6.5	−30.5	−37.3
175	210 vs. 160	30	49.0	−9.7	0	43.7	67.8	57.0
		40	62.7	−17.8	0	53.0	75.5	68.0

disclosed by Jiménez-García et al. [23].

Data provided in Fig. 9a suggests that the refrigeration loop in the baseline configuration reduces around 30 % of the total destroyed exergy generated by the refrigeration system. The data highlights that the air-cooled absorber component of the refrigeration loop produces the highest exergy destruction, followed by the evaporator and condenser as mentioned in Refs. [25–28]. In addition, the analysis indicates a decrease in the refrigeration system's exergy efficiency with an increase in T_{amb}. As displayed in Fig. 9a, there is a reduction in exergy destruction by the evaporator and absorber, compared to that of the condenser, as the ambient temperature increases. This trend is consistent with the observations made during an increase in ΔP_{val1}. Moreover, the figure suggests a decline in overall exergy destruction in the refrigeration system, attributed mainly to a decrease in system cooling capacity with an increase in T_{amb}.

Fig. 9b demonstrates that the customised refrigeration system destroys greater exergy than the baseline configuration displayed in Fig. 9a, due to the increased cooling capacity. It is noteworthy that approximately 40 % of total exergy destruction in the customised configuration is contributed by the refrigeration loop, which negatively affects the remaining refrigeration system components. This emphasises the substantial influence of an elevated $T_{cf,hot}$. The most notable aspect is the rise in the condenser's contribution, coupled with the decline in exergy efficiency.

4. Conclusions

This study presents a comprehensive analysis of the heat and mass transfer processes in an ammonia and water air-cooled absorption system. The ROBUR® ACF60-00 LB model employs hot water temperatures ranging from 160 °C to 210 °C. The system was analysed under ambient temperatures ranging from 15 °C to 40 °C. The goal of this investigation is to reduce the refrigeration system's size, particularly in off-design conditions and high ambient temperatures, thereby improving the usage of the air-cooled absorber and condenser across the chiller's operating range.

The proposed methodology entails adjusting the high-pressure level of the absorption chiller by altering the pressure drop in valve 1 situated right after the condenser. To achieve this objective, a modular differential mathematical model has been developed, which is based on mass, species, and energy balance. The model's development relied on local heat and mass transfer coefficients. The thermal conductance of the main components in the refrigeration system was considered as unknown and was determined through calculations. To validate the model's results, data published by the manufacturer and documented in the literature were utilised.

The implemented model presents an assessment tool for identifying the minimum required size of the air-cooled absorber and

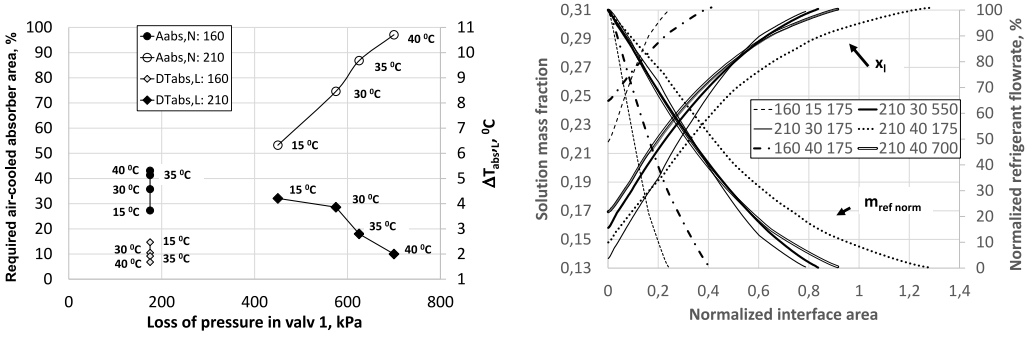

Fig. 7. Air-cooled absorber: a) minimum required area, normalised with its geometric area, $A_{abs,N}$, b) local solution mass fraction and refrigerant flowrate, normalised with $\dot{m}_{ref}$. Box: feed hot water temperature, ambient temperature, °C; and ΔP_{valv1}, in kPa, in the baseline and in the custom configurations. Box: feed hot water temperature, °C.

Table 7
Air-cooled condenser. Comparative results, expressed in %.

$\Delta P_{val\ 1}$, kPa	$T_{cf,hot,}$ °C	$T_{amb,}$ °C	$\Delta\dot{m}_{ref}$	$\Delta\Delta T_{cf,cond,L}$	ΔUA_{cond}	ΔA_{cond}	$\Delta\Delta T_{cf,\ cond,G}$	$\Delta\varepsilon_{cond}$
$\Delta P_{val\ 1L}$ vs. 175	210	30	−12.9	84.1	−87.0	−260.8	−18.3	0
		40	−18.5	87.8	−90.1	−316.8	−25.7	0
175	210 vs. 160	30	49.0	−44.9	72.5	72.7	50.5	0
		40	62.7	−54.1	82.8	83.1	63.3	0

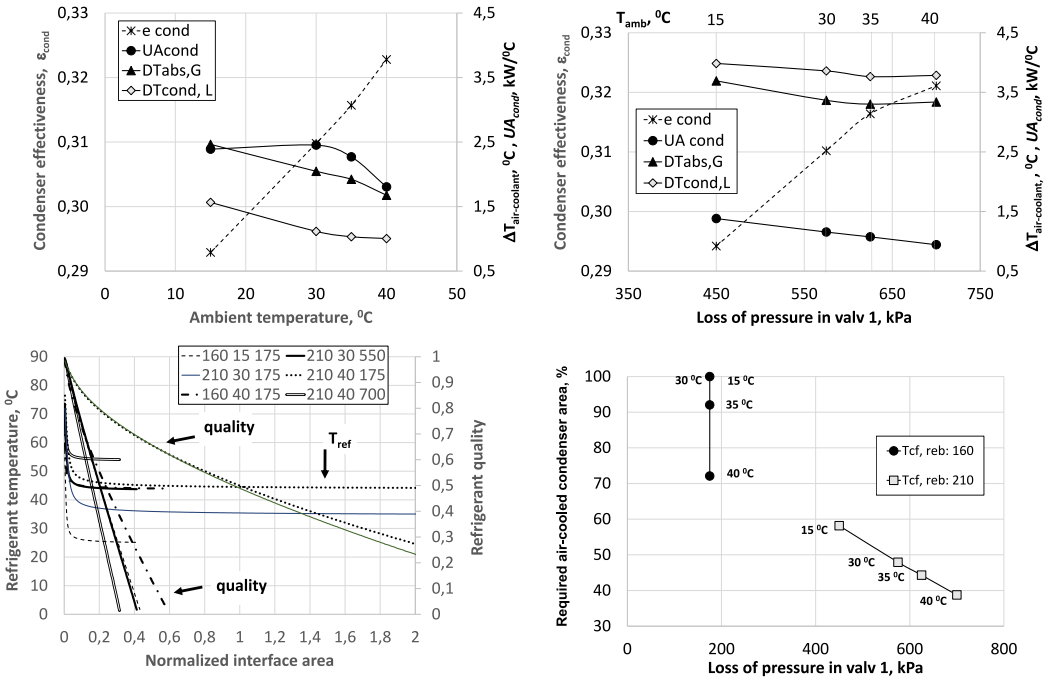

Fig. 8. Condenser: effectiveness, thermal conductance, global and local temperature increase in air-coolant flow, a) in the baseline and b) customised configurations, c) in local solution and the temperature of the refrigerant. Box: feed hot water temperature, ambient temperature, °C; and ΔP_{valv1}, in kPa. d) Minimum required area, normalised with its geometrical area, in the baseline and in the customised configurations. Box: feed hot water temperature, °C.

Table 8
Exergy destruction: Contribution to the air-cooled absorber, condenser, evaporator, and refrigeration loop to the refrigeration system. Exergy efficiency. Comparative results, expressed in %.

$\Delta P_{val\ 1}$, kPa	$T_{cf,hot,}$ °C	T_{amb}, °C	ΔI_{abs}	ΔI_{cond}	ΔI_{evap}	$\Delta I_{ref\ loop}$	$\Delta \eta_{ex}$
$\Delta P_{val\ 1L}$ vs. 175	210	30	3.2	22.5	−20.1	−2.9	−8.0
		40	5.7	26.1	−24.1	−4.3	−7.4
175	210 vs. 160	30	7.4	21.1	48.1	21.7	−6.9
		40	8.2	23.7	63.5	33.3	−7.9

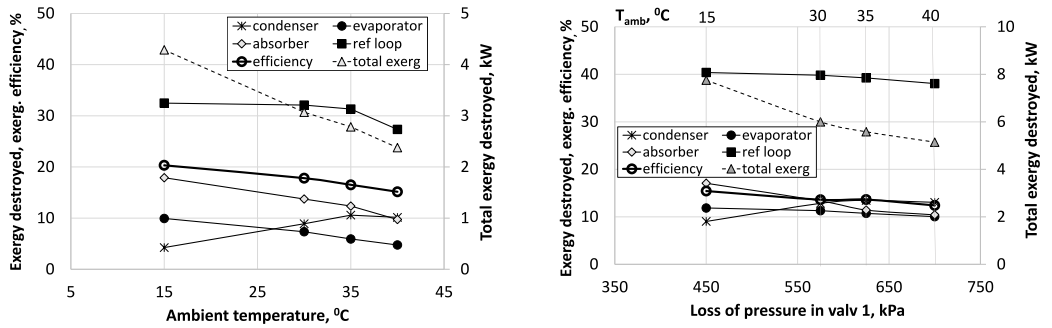

Fig. 9. Contribution to exergy destruction: air-cooled absorber, condenser, evaporator, and refrigerant loop, %, exergy efficiency, %, and total exergy destroyed in the refrigeration system, kW, a) in the baseline and b) in the customised configuration.

condenser when organized in a series configuration, and while in partial chiller operation under this scheme.

The analysis results show that a pressure loss increase in valve 1 leads to higher high- and low-pressure levels. Specifically, it is revealed that at a hot feed water temperature of 210 °C and an ambient temperature of 40 °C, an increase in pressure loss from 175 to 2246 kPa in valve 1 causes the

- Air-cooled absorber to reduce its nominal size by 37.3 %.
- a reduction of 37.3 % in the size of the air-cooled absorber, A_{abs}. Note that the decreases in $\dot{m}_{ref}$ is 18.5 %, which is less than that of A_{abs}.
- Air-cooled condenser size to decrease by 3.1 times.
- Circulation factor to rise from 4.5 to 5.5. Consequently, $\dot{m}_{cf\ evap}$ regulation is required to optimize tunning between $\dot{m}_{cf\ evap}$ and $\dot{m}_{ref}$.
- The contribution of condenser to exergy destruction to increase up to 26.1 %.
- The contribution of the evaporator to exergy destruction to reduce up to 24.1 %.

Despite the increase in the pressure levels, the effectiveness of the evaporator, air-cooled absorber, and condenser is hardly affected. Hence, adjusting the pressure levels in an air-cooled ammonia-water absorption chiller by elevating ΔP_{valv1} during high ambient temperature and high feed water temperature is an effective method of reducing the size of the air-cooled absorber. The results show that the increase in the condenser's contribution to exergy destruction is offset by the decrease in the evaporator's contribution. Regulation of the chilled water flow rate is also required.

Funding

This work has been developed in the frame of the ASTEP project, funded by the European Union's Horizon 2020 research and innovation program under grant agreement No 884411 and the ACES2030-CM project, funded by the Regional Research and Development in Technology Program 2018 (ref. P2018/EMT-4319).

Author agreement statement

Maria Esther Palacios Lorenzo (Corresponding Author) and Daniel Marcos del Cano (Coauthor) declare that this manuscript is original, has not been published before and is not currently being considered for publication elsewhere. We confirm that the manuscript has been read and approved by all named authors and that there are no other persons who satisfied the criteria for authorship but are not listed. We further confirm that the order of authors listed in the manuscript has been approved by all of us. We understand that the Corresponding Author is the sole contact for the Editorial process. She is responsible for communicating with the other authors about progress, submissions of revisions and final approval of proofs.

CRediT authorship contribution statement

María Esther Palacios-Lorenzo: Conceptualization, Data curation, Formal analysis, Investigation, Methodology, Software, Supervision, Validation, Visualization, Writing – original draft, Writing – review & editing. **José Daniel Marcos:** Conceptualization, Funding acquisition, Methodology, Project administration, Writing – review & editing.

Declaration of competing interest

The authors declare that they have no known competing financial interests or personal relationships that could have appeared to influence the work reported in this paper.

Data availability

Data will be made available on request.

Nomenclature

AbbreviationsSymbols

a_{int}	specific interfacial area, m^2/m^3
A	area transfer, m^2
A_a	active area of the tray, m^2
A_d	downcomer area, m^2
A_h	hole area of the tray, m^2
A_h/A_t	fractional free area
A_t	tower cross-section area, m^2
D	tube diameter, m
d_h	hole diameter of the tray in the distillation column, m^2
e	wall thickness, m
e_{tray}	tray spacing in the distillation column, m
e_M	Murphree vapour plate efficiency
f	circulation ratio, $\dot{m}_{dR}/\dot{m}_{ref}$
F	mass transfer coefficient, kmol/(m^2 s)
h_f	reboiler length, m

h	specific enthalpy, kJ/kg
h_t	heat transfer coefficient, W/(m^2 K)
h_f	fin length, m
$\dot{n}$	molar flux, kmol/(m^2 s)
$\dot{m}$	mass flow rate, kg/s
P	pressure, kPa
$\dot{Q}$	heat flow, W
s	fin pitch, m
T	temperature, °C
t_m	fin thickness, m
U	overall heat transfer coefficient, W/(m^2 K)
x	mass fraction
z	ratio of ammonia to the total molar flux

Subscripts and superscripts

abs	air-cooled absorber
air	coolant air
cabs	solution-cooled absorber
cond	air-cooled condenser
cf	coupling fluid
dP	dilute solution in ammonia
dR	concentrate solution in ammonia
e	at thermodynamic equilibrium
evap	evaporator
reb	reboiler
rect	solution-cooled rectifier
ref	refrigerant

References

[1] UN United Nations, World population prospects — population division, Available online: https://population.un.org/wpp/. (Accessed 9 July 2023).
[2] A. Almasri, N.H. Abu-Hamdeh, K.K. Esmaeil, S. Suyambazhahan, Thermal solar sorption cooling systems - a review of principle, technology, and applications, Alex. Eng. J. 61 (2022) 367–402, https://doi.org/10.1016/j.aej.2021.06.005.
[3] M. Herrando, R. Simon, I. Guedea, N. Fueyo, The challenges of solar hybrid PVT systems in the food processing industry, Appl. Therm. Eng. 184 (2021), 116235, https://doi.org/10.1016/j.applthermaleng.116235.
[4] K.E. Herold, R. Radermacher, S.A. Klein, Absorption Chillers and Heat Pumps, second ed., CRC Press, 2016.
[5] S.M. Alelyani, N.W. Fette, E.B. Stechel, P. Doron, P.E. Phelan, Techno-economic analysis of combined ammonia-water absorption refrigeration and desalination, Energy Convers. Manag. 143 (2017) 493–504, https://doi.org/10.1016/j.enconman.2017.03.085.
[6] A.E. Zohir, E.S. Ali, A.M. Farid, R.N. Elshaer, R.H. Mohammed, A.S. Alsaman, H.H. El-Ghetany, A.A. Askalany, A state-of-the-art of experimentally studied adsorption water desalination systems, Int. J. Energy Environ. 14 (2023) 573–599, https://doi.org/10.1007/s40095-022-00536-y.
[7] J. Cano-Nogueras, J. Muñoz-Antón, J.M. Martinez-Val, A new thermal-solar field configuration: the rotatory Fresnel collector or sundial, Energies 14 (2021) 4139, https://doi.org/10.3390/en14144139.
[8] A.M. Abed, M.A. Alghoul, K. Sopian, H. Sh Majdi, A.N. Al-Shamani, A.F. Muftah, Enhancement aspects of single absorption cooling cycle: a detailed review, Renewable Sustainable Energy Rev. 77 (2017) 1010–1040, https://doi.org/10.1016/j.rser.2016.11.231.
[9] X. Tao, D. Thanganadar, K. Patchigolla, Compact ammonia/water absorption chiller of different cycle configurations: parametric analysis based on heat transfer performance, Energies 15 (2022) 6511, https://doi.org/10.3390/en15186511.
[10] H.K. Mukhtar, S. Ghani, Improving the performance of a commercial absorption cooling system by using ejector: a theoretical study, Case Stud. Therm. Eng. 45 (2023), 102967, https://doi.org/10.1016/j.csite.2023.102967.
[11] L. Yang, K. Du, S. Bao, Y. Wu, Investigations of selection of nanofluid applied to the ammonia absorption refrigeration system, Int. J. Refrig. 35 (2011) 2248–2260, https://doi.org/10.1016/j.ijrefrig.2012.08.003.
[12] S. Libotean, D. Salavera, M. Valles, X. Esteve, A. Coronas, Vapor-liquid equilibrium of ammonia + lithium nitrate + water and ammonia + lithium nitrate solutions from (293.15 to 353.15) K, J. Chem. Eng. Data 52 (2007) 1050–1055, https://doi.org/10.1021/je7000045.
[13] A. Altamirano, N.L. Pierrès, B. Stutz, Review of small-capacity single-stage continuous absorption systems operating on binary working fluids for cooling: theoretical, experimental and commercial cycles, Int. J. Refrig. 106 (2019) 350–373, https://doi.org/10.1016/j.ijrefrig.2019.06.033.
[14] A. Goyal, M.A. Staedter, D.C. Hoysall, M.J. Ponkala, S. Garimella, Experimental evaluation of small-capacity waste-heat driven ammonia-water absorption chiller, Int. J. Refrig. 79 (2017) 89–100, https://doi.org/10.1016/j.ijrefrig.2017.04.006.
[15] M.A. Staedter, S. Garimella, Development of a micro-scale heat exchanger based, residential capacity ammonia–water absorption chiller, Int. J. Refrig. 89 (2018) 93–103, https://doi.org/10.1016/j.ijrefrig.2018.02.016.
[16] P. Hrnjak, A.D. Litch, Microchannel heat exchangers for charge minimization in air-cooled ammonia condensers and chillers, Int. J. Refrigerat. 31 (2008) 658–668. https://doi:10.1016/j.ijrefrig.2007.12.012.
[17] S. Garimella, R.N. Christensen, D. Lacy, Performance evaluation of a generator-absorber heat-exchanger heat-pump, Appl. Therm. Eng. 16 (1996) 591–604.
[18] C.A. Infante-Ferreira, Vertical Tubular Absorber for Ammonia-Salt Absorption Refrigeration, PhD, 1987.
[19] J. Fernández-Seara, F.J. Uhía, J. Sieres, Analysis of an air-cooled ammonia–water vertical tubular absorber, Int. J. Therm. Sci. 46 (2007) 93–103, https://doi.org/10.1016/j.ijthermalsci.2006.03.005.
[20] J. Fernández-Seara, J. Sieres, C. Rodríguez, M. Vázquez, Ammonia–water absorption in vertical tubular absorbers, Int. J. Therm. Sci. 44 (2005) 277–288, https://doi.org/10.1016/j.ijthermalsci.2004.09.001.

[21] J. Sieres, J. Fernández-Seara, Modelling of simultaneous heat and mass transfer processes in ammonia-water absorption systems from general correlations, Heat Mass Tran. 44 (2007) 113–123, https://doi.org/10.1007/s00231-006-0226-3.
[22] J. Fernandez-Seara, J. Sieres, The importance of the ammonia purification process in ammonia–water absorption systems, Energy Convers. Manag. 47 (2006) 1975–1987, https://doi.org/10.1016/j.enconman.2005.09.002.
[23] S. Garimella, M.J. Ponkala, A. Goyal, M.A. Staedter, Waste-heat driven ammonia-water absorption chiller for severe ambient operation, Appl. Therm. Eng. 154 (2019) 442–449, https://doi.org/10.1016/j.applthermaleng.2019.03.098.
[24] S. Garimella, D.M. Forinash, D.B. Boman, Air-cooled absorbers for extreme-ambient absorption heat pumps, Int. J. Refrig. 120 (2020) 260–270, https://doi.org/10.1016/j.ijrefrig.2020.08.023.
[25] S. Chakraborty, G. Kini, S. Garimella, Novel geometries for air-cooled condensation of ammonia-water mixtures, Int. J. Refrig. 121 (2021) 183–192, https://doi.org/10.1016/j.ijrefrig.2020.10.010.
[26] G. Moreno-Quintanar, V. Gomez, R. Best, Exergetic analysis of a GAX refrigeration system design to operate with LP gas and solar energy, Energy Proc. 70 (2015) 644–651.
[27] J.C. Jiménez-García, W. Rivera, Exergy analysis of an experimental ammonia/water absorption cooling system, Case Stud. Therm. Eng. 49 (2023), 103167, https://doi.org/10.1016/j.csite.2023.103167.
[28] A.M. Blanco-Marigorta, J.D. Marcos, Key issue on the exergy analysis of H_2O/LiBr absorption cooling systems, Case Stud. Therm. Eng. 28 (2021), 101568, https://doi.org/10.1016/j.csite.2021.101568.
[29] G. Grossman, A. Zaltash, ABSIM- modular simulation of advanced absorption systems, Int. J. Refrig. 24 (2001) 531–543.
[30] J.J. Pereira, C.A. Cabral, C. Almir, J. Batista, A.A. Ochoa, J.C. Charamba, Energetic analysis of a commercial absorption refrigeration unit using an ammonia-water mixture, Acta Sci. Technol. 39 (2017) 439–448, https://doi.org/10.4025/actascitechnol.v39i4.29904.
[31] J. Sieres, J. Fernandez-Seara, Evaluation of the column components size on the vapour enrichment and system performance in small power NH_3–H_2O absorption refrigeration machines, Int. J. Refrig. 29 (2006) 579–588, https://doi.org/10.1016/j.ijrefrig.2005.10.004.
[32] H.T. Chua, H.K. Toh, K.C. Ng, Thermodynamic modelling of an ammonia–water absorption chiller, Int. J. Refrig. 25 (2002) 896–906.
[33] A.K. Coker, Ludwing's Applied Process Design for Chemical and Petrochemical Plants, fourth ed., Elsevier, 2010.
[34] O.M. Ibrahim, S.A. Klein, Thermodynamic Properties of Ammonia-Water Mixtures, ASHRAE Transactions. Symposia, 1993, pp. 1495–1502.
[35] R.M. Lazzarin, A. Gasparella, G.A. Longo, Ammonia-water absorption chiller for refrigeration: theoretical and real performances, Int. J. Refrig. 19 (1996) 239–246.
[36] F. Taboas, M. Valles, M. Bourouis, A. Coronas, Pool boiling of ammonia/water and its pure components: comparison of experimental data in the literature with the predictions of standard correlations, Int. J. Refrig. 30 (2007) 778–788, https://doi.org/10.1016/j.ijrefrig.2006.12.009.
[37] T. Morosuk, G. Tsatsaronis, A new approach to the exergy analysis of absorption refrigerant machines, Energy 33 (2008) 890–907, https://doi.org/10.1016/j.energy.2007.09.012.
[38] A.F. Mills, Transferencia de Calor, McGrawHill, first ed., 1999.
[39] V.D.I. Wärmeatlas, VDI Heat Atlas, second ed., Springer, 2010.
[40] N.A.A. Qasem, S.M. Zubair, Compact and microchannel heat exchangers: a comprehensive review of airside friction factor and heat transfer correlations, Energy Convers. Manag. 173 (2008) 555–601, https://doi.org/10.1016/j.enconman.2018.06.104.
[41] D. Barnea, A unified model for prediction flow-pattern transition from the whole range of pipe inclinations, Int. J. Multiphas. Flow 13 (1987) 1–12.
[42] L. Yi-ping, Z. Hua, W. Shu-hua, W. Jing, Gas–liquid interfacial friction factor for the transition from stratified to slug flow, Microgravity Sci. Technol. 20 (2008) 299–305, https://doi.org/10.1007/s12217-008-9078-4.
[43] R.N. Hassanlouei, H. Firouzfar, N. Kasiri, M.H. Khanof, A simple mathematical model for slug liquid holdup in horizontal pipes, Sci Iranica C 19 (2012) 1653–1660, https://doi.org/10.1016/j.scient.2012.05.010.
[44] P.L. Sppeding, N.P. Hand, Prediction in stratified gas-liquid co-current flow in horizontal pipelines, Int. J. Heat Mass Tran. 40 (1997) 1923–1935.
[45] D. Barnea, N. Brauner, Holdup of the liquid slug in two phase intermittent flow, Int. J. Multiphas. Flow 11 (1985) 43—49.
[46] F.A. Franca, A.C. Bannwart, R.M.T. Camargo, M.A.L. Goncalves, Mechanistic modelling of the convective heat transfer coefficient in gas-liquid intermittent flows, Heat Tran. Eng. 29 (2008) 984–998, https://doi.org/10.1080/01457630802241091.
[47] E. Al-Safran, Investigation and prediction of slug frequency in gas/liquid horizontal pipe flow, J. Petrol. Sci. Eng. 69 (2009) 143–155, https://doi.org/10.1016/j.petrol.2009.08.009.
[48] D. He, S. Chen, B. Bai, Void fraction measurement of stratified gas-liquid flow based on multi-wire capacitance probe, Exp. Therm. Fluid Sci. 102 (2019) 61–73, https://doi.org/10.1016/j.expthermflusci.2018.11.005.
[49] D.S. Scott, W. Hayduk, Gas Absorption in Horizontal Cocurrent Bubble Flow, The Canadian J Chem Eng, 1996, pp. 130–136.
[50] J.W. Ciborowski, R.M. Rychlicki, Mass transfer in two-phase gas-liquid wavy flow, Int. J. Heat Mass Tran. (1971) 1261–1274.
[51] S. Klein, A Model of the Steady-State Performance of an Absorption Heat Pump, US Department of Commerce, 1992, pp. 82–2602. QC 100.U56.